Science Advances

AAAS

Supplementary Materials for

Extensive marine anoxia during the terminal Ediacaran Period

Feifei Zhang, Shuhai Xiao, Brian Kendall, Stephen J. Romaniello, Huan Cui, Mike Meyer, Geoffrey J. Gilleaudeau, Alan J. Kaufman, Ariel D. Anbar

The PDF file includes:

- fig. S1. Simplified schematic representation of the major source and sinks of U in the modern ocean along with their isotopic compositions (sources) or associated isotopic fractionations (sinks) [modified after Tissot and Dauphas (*54*) and Wang *et al.* (*55*)].
- fig. S2. Geochemical profiles for the study sections.
- fig. S3. Petrographic images of the Hamajing Member.
- fig. S4. Petrographic images of the Shibantan Member.
- fig. S5. Petrographic images of the Baimatuo Member and the Yanjiahe Formation.
- fig. S6. Chemostratigraphic profiles of $\delta^{238}U$, Sr content, Mn content, Mn/Sr ratio, and $\delta^{18}O$ for the study sections.
- fig. S7. Chemostratigraphic profiles of $\delta^{238}U$, Mn/(Mg + Ca) ratio, and Sr/(Mg + Ca) ratio for the study sections.
- fig. S8. Cross-plots of $\delta^{13}C$-$\delta^{18}O$ for the study sections.
- fig. S9. Chemostratigraphic profiles of $\delta^{238}U$, Al content, Rb/Sr ratio, U/Al ratio, and Mg/Ca molar ratio for the study sections.
- fig. S10. Chemostratigraphic profiles of U and Mo concentrations, Ce anomalies, U/(Mg + Ca) ratio, and Mo/(Mg + Ca) ratio for the study sections.
- fig. S11. Mass balance modeling calculations show variations of seawater $\delta^{238}U$ values as a function of anoxic/euxinic seafloor area while keeping Δ_{anoxic} constant (+0.6‰) and testing various suboxic areal extents.
- fig. S12. Calculated combination f_{anoxic} and $f_{suboxic}$ to account for latest Ediacaran seawater average $\delta^{238}U$ of −0.95‰.
- table S1. The sample-dissolving procedure.

- table S2. Cross-correlation coefficients (R^2) and P values calculated to test the influence of diagenetic indicators on $\delta^{238}U$ (confidence interval, 95%).
- table S3. Summary of the parameters used in the modeling excise.
- References (*54–100*)

Other Supplementary Material for this manuscript includes the following:
(available at advances.sciencemag.org/cgi/content/full/4/6/eaan8983/DC1)

- database S1 (Microsoft Excel format). $\delta^{238}U$ data with associated geochemical data at the Wuhe section.
- database S2 (Microsoft Excel format). $\delta^{238}U$ data with associated geochemical data at the Gaojiashan section.
- database S3 (Microsoft Excel format). Analytical results of standard summary (Wuhe measurements).
- database S4 (Microsoft Excel format). Analytical results of standard summary (Wuhe measurements).

Mass balance description of uranium isotope in the ocean

Uranium is a redox-sensitive trace metal with a residence time of ~500 kyr in the modern ocean (*22, 56*). Uranium occurs in two redox states in natural waters: soluble U(VI) under oxygenated conditions and insoluble U(IV) under anoxic conditions. Isotope fractionation between U(IV) and U(VI) is driven by the dominance of nuclear volume effects (*25, 44*). As a result, during reduction of U(VI) to U(IV), the reduced U(IV) is enriched in the heavier [238]U isotope, thus enriching the remaining dissolved U(VI) reservoir in the lighter [235]U isotope. This is observed in the Black Sea (*24, 42, 57*). Microbially-mediated reduction of U(VI) to U(IV) under anoxic conditions is associated with a large isotopic fractionation ranging between 0.68 ‰ and 0.99 ‰ (*26, 27, 58*).

The only major source of U to the ocean is oxidative mobilization of U from the upper continental crust and transport of dissolved U(VI) to the oceans via rivers. The $\delta^{238}U$ value of dissolved U in rivers is dominated by the U concentration and $\delta^{238}U$ of the source lithologies (*59*). The estimated average $\delta^{238}U$ of the world's major rivers ranges between –0.26 ‰ and –0.34 ‰ (*59–61*), which reflects the estimated average $\delta^{238}U$ of the continental crust [−0.30 ± 0.04 ‰ (2σ), (*60*); −0.31 ± 0.05 ‰ (2σ), (*54*)]. In our U isotope modeling calculation below, we adopted a riverine $\delta^{238}U$ of –0.34 ‰.

There are multiple sinks for U in the ocean. The major sinks are sediments deposited beneath anoxic/euxinic bottom waters, sediments deposited beneath weakly oxygenated bottom waters, and marine carbonates (*22, 54, 62*). Minor sinks include ferromanganese oxides and the hydrothermal alteration of oceanic crust (*22, 54, 62*). The largest expression of U isotope fractionation (~0.4 ‰ to ~1.2 ‰) in the marine environment occurs during U burial in anoxic/euxinic sediments, like those of the Black Sea, the Saanich Inlet, and the Framvaren Fjord (*23, 41, 42, 63, 64*). By contrast, the fractionation of U isotopes during removal to suboxic sediments is only ~0.1 ‰ based on observations from the Peruvian continental margin and off the coast of Washington State, where sediments underlying weakly oxygenated waters have an average $\delta^{238}U$ of –0.28 ± 0.19 ‰ (*23*) and –0.23 ± 0.19‰ (*59*), respectively. Both natural and laboratory observations suggest at most a small offset between the $\delta^{238}U$ of primary carbonate precipitates and seawater (*23, 24, 29, 39, 65*). Sedimentary carbonates may incorporate U(IV) from sulfidic pore waters, leading to values that are 0.2–0.4 ‰ higher compared with seawater, although this process can potentially be monitored by examining local depositional redox conditions where the carbonates precipitated (*29*). The fractionation of U isotopes during removal to Mn nodules and metalliferous sediments is –0.24 ‰, and is well constrained by both natural samples (*55, 66*) and adsorption experiments (*67*). Seafloor alteration at high temperatures is assumed to have no isotope fractionation, and seafloor alteration at low temperatures is estimated to have a fractionation factor of 0.25 ‰ (*54*).

Non-anoxic sinks and the associated fractionation factors

A simplified schematic representation of the major source and sinks of U in the modern ocean along with their isotopic compositions (sources) or associated isotopic fractionations (sinks) is presented in fig. S1 (modified after Wang *et al*. (*55*) and Tissot *et al*. (*54*)). In order to simplify our mass balance calculations, several types of sinks are

lumped into a single oxic sink, including Fe-Mn crusts, pelagic clays, low temperature and high temperature oceanic crust alteration, marine carbonates, and coastal retention. Additionally, the oxic sink and suboxic sink are lumped together into a single "other" sink to make the estimation of U removal associated with anoxic/euxinic sinks solvable. The overall U isotope fractionation factor for the oxic sink and the "other" sink are calculated as a weighted average of the fractionation factors for the individual components. The fractionation factors between the oxic sink and seawater and between the "other" sink and seawater are 0.01 ‰ (Δ_{oxic}) and 0.04 ‰ (Δ_{other}), respectively.

Geological background of the studies sites

The geological and stratigraphic background of the Dengying Formation in the Yangtze Gorges area was detailed in Chen *et al*. (*68*) and was summarized by Meyer *et al*. (*32*). To briefly summarize, the upper Ediacaran Dengying Formation overlies the lower–middle Ediacaran Doushantuo Formation and underlies the Yanjiahe Formation, which contains the Ediacaran–Cambrian boundary (*69*). The Dengying Formation was deposited on a shallow marine carbonate platform in an inner shelf environment (*70*), and its age is constrained between 551.1±0.7 Ma and ~541 Ma based on available radiometric dates and stratigraphic correlations (*9, 30, 71*). The Dengying Formation is divided into three members. These are the Hamajing, Shibantan, and Baimatuo members from bottom to top (fig. S2 in the supplementary information and Fig. 1 in the main text). The Hamajing Member consists of peritidal dolostone. The Shibantan Member is composed of dark gray, thin-bedded, bituminous limestone interpreted to have been deposited in a subtidal environment (*72*). The Baimatuo Member is composed of light gray, massive peritidal dolostone (*68, 72*).

The geological and stratigraphic background of the Dengying Formation in the Gaojiashan area was detailed in Cai *et al*. (*33*) and Cui *et al*. (*31*). To briefly summarize, the study area is located in the northwestern margin of the Yangtze Platform. Ediacaran successions in the Gaojiashan area consist of the Doushantuo and the Dengying formations, similar to classical Ediacaran successions in the southeastern margin of the Yangtze Platform. The Dengying Formation is divided into three members. These are the Algal Dolomite, Gaojiashan, and Beiwan members from bottom to top, which are typically correlated to the Hamajing, Shibantan, and Baimatuo members, respectively, in the Three Gorges area. The Algal Dolomite Member is characterized by light gray, peritidal dolostone. The overlying Gaojiashan Member is characterized by thin-bedded, subtidal, fossiliferous calcisiltite-siltstone and mudstone with limestone interbeds. Microbial laminae and rip-up clasts are common in limestones of the upper Gaojiashan Member, which is capped by a thick sandstone bed. The overlying Beiwan Member consists of thick-bedded, peritidal dolostone with stromatactis-like structures and *Cloudina* fossils. The studied Gaojiashan Member is 55 m thick and can be divided into three units. The lower Gaojiashan Member is characterized by 19 m of greenish and brownish siltstone, greenish silicified tuffaceous siltstone, and silty shale. The middle Gaojiashan Member consists of 8 m of non-fossiliferous, interbedded calcisiltite-siltstone and calcilutite-mudstone, followed stratigraphically up-section by 12 m of fossiliferous calcisiltite-siltstone–calcilutite-mudstone interbeds that contain abundant pyritized fossils

(*Conotubus and Gaojiashania*), calcareous microfossils (*Protolagena*), and horizontal trace fossils towards the upper part of this unit. In the succeeding 14 m of strata up-section, limestone becomes increasingly dominant over siltstone, fossils become increasingly scarce and are dominated by *Cloudina*, but wrinkled microbial sedimentary structures and rip-up clasts are common.

Evaluation of carbonate diagenesis

Marine carbonate sediments can faithfully record chemical signatures of seawater provided that post-depositional processes have not caused significant alteration. To assess diagenesis, we used a combination of sedimentary petrography and standard geochemical criteria. Specifically, we compared our U isotope data to standard diagenetic indicators such as Mn content, Sr content, Mn/Sr ratios, and O isotope composition to evaluate the influence of meteoric or burial fluids on preserved U isotope signatures.

To provide a framework for our interpretation, we briefly summarize the way in which petrography and geochemistry can be used to assess diagenesis (after Gilleaudeau *et al*. (*73*)). Broadly, grain size and the degree of preservation of primary textural features can be indicative of fluid composition during diagenesis. Fabric-retentive micritic to microsparitic fabrics that preserve original textural details indicate that recrystallization occurred in the presence of fluids similar in composition to seawater, leading to the inference that diagenesis was early—either synsedimentary or during shallow burial. Dolomitization may also occur during early diagenesis in the presence of seawater-buffered fluids, resulting in a high degree of fabric retention. By contrast, diagenesis in the presence of fluids very different in composition than seawater (meteoric or deep burial fluids) commonly results in crystal coarsening and destruction of primary textural details. Altered carbonate phases (both calcite and dolomite) are often sparry and characterized by planar grain boundaries.

The isotopic composition of oxygen can also be altered during diagenesis, and because of the high concentration of oxygen in diagenetic fluids, the oxygen isotopic composition of carbonate minerals will be reset at relatively low water/rock ratios (< 10; (*34, 74*)). Diagenetic alteration tends to decrease $\delta^{18}O$ values, although the oxygen isotopic composition of meteoric fluids is highly variable depending on geographic location (*75*). Compilation of data for petrographically well-preserved Proterozoic carbonate phases indicates $\delta^{18}O$ values generally > −9 ‰ (*76, 77*), although Kaufman and Knoll (*78*) suggested that values > −5 ‰ may be a more reliable indicator of relatively pristine oxygen isotope compositions in Neoproterozoic settings. These values can be used as an initial benchmark for assessing diagenesis.

Trace elements (Sr, Mn, and Fe) substituted into the lattice of carbonate minerals can also be used as diagenetic indicators. The incorporation of trace elements into the carbonate lattice is governed by the distribution coefficient, and different types of diagenetic fluids have different trace element compositions. Modern, well-oxygenated seawater is high in Sr relative to Mn and Fe such that primary precipitates and early diagenetic phases formed in the presence of seawater are generally enriched in Sr relative to Mn and Fe

(*74*). This is particularly true for aragonite because of the high distribution coefficient for Sr into aragonite compared to other carbonate minerals (*79*). Early fabric-retentive dolostone can also be enriched in Sr relative to Mn and Fe, although dolomite generally has a lower preference for Sr (*80*) and a higher preference for Mn and Fe (*81*) compared to calcite.

Meteoric and burial fluids, by contrast, tend to be depleted in Sr relative to seawater (*74*). The recrystallization process also acts to expel Sr from the lattice of carbonate minerals because of its relatively large ionic radius compared to Ca (*82*). As a result, meteoric or burial diagenetic phases are often depleted in Sr relative to precursor marine phases. Burial fluids can also be substantially enriched in Mn and Fe, particularly under reducing conditions (*79*). This commonly leads to Mn and Fe enrichment in burial diagenetic phases. Meteoric fluids are variable in their Mn and Fe content—depending largely on redox conditions—such that meteoric calcite phases can be characterized by enrichment or depletion of Mn and Fe.

These general relationships have led to the establishment of traditional criteria such as Mn/Sr ratio to assess the fidelity of primary geochemical signatures in carbonate rocks. For example, Kaufman and Knoll (*78*) suggested that both limestone and dolostone with Mn/Sr ratios < 10 can be expected to retain their primary carbon isotopic signatures. In this study, we use a conservative Mn/Sr ratio of 2.5 as a benchmark for assessing diagenesis.

For the Hamajing Member at Wuhe, we examined four thin sections and we provide photomicrographs of samples HMJ-14 and HMJ-19 at various magnifications in fig. S3. Overall, the Hamajing Member is comprised of relatively homogeneous micritic to microsparitic fabric-retentive dolomite with volumetrically insignificant veins and small voids filled with dolomite spar. For the overlying Shibantan Member, we examined ten thin sections and we provide photomicrographs of samples SBT-26, SBT-42, SBT-89, and SBT-107 at various magnifications in fig. S4. The Shibantan Member is composed of micritic to microsparitic calcite that is fabric-retentive, preserving primary textural features such as thin, microbial laminations. Strata are generally organic-rich and preserve alternating organic-poor and organic-rich mm-scale laminations, as well as occasional intervals with small, dispersed mud clasts. For the Baimatuo Member, we examined four thin sections and we provide photomicrographs of samples BMT-172, BMT-186, and BMT-200 in fig. S5A-C. In the Baimatuo Member, dolomite microspar is also fabric-retentive, preserving primary mm-scale laminations and small mud rip-up clasts. Lastly, for the Yanjiahe Formation that sits above the Dengying Formation, we examined five thin sections and we provide photomicrographs for samples YJH-2, YJH-21, and YJH-40 in fig. S5D-F. Limestone of the Yanjiahe Formation is composed of micritic to microsparitic calcite that is generally fabric-retentive. Some intervals are organic-rich and preserve thin, microbial laminations. Intraformational conglomerates composed of sub-mm-scale mud rip-up clasts are common.

In summary, none of the samples examined in this study show the degree of recrystallization observed by Hood *et al.* (*36*) in the Neoproterozoic Balcanoona reef

complex, South Australia. The generally fabric-retentive nature of our samples is suggestive of primary marine precipitation or early stage diagenesis in the presence of seawater (*e.g.*, (*83, 84*)).

With respect to geochemical characteristics, the Hamajing Member is characterized by relatively low Mn concentrations (< 100 ppm with the exception of two samples), as well as relatively low Sr concentrations (< 100 ppm). Mn/Sr ratios are < 2, with the exception of two samples that have been excluded from further consideration (fig. S6). Relatively low Sr concentrations are not uncommon in early fabric-retentive dolostone, and therefore are not taken to indicate late-stage diagenetic alteration. Oxygen isotope values are > −6 ‰, which also argues against late-stage diagenesis. In summary, petrographic, trace element, and isotopic characteristics suggest that the Hamajing Member has the potential to record seawater geochemical signatures.

In the Shibantan Member, Mn concentrations are exceptionally low (< 15 ppm) and Sr concentrations are strongly elevated (up to ~2,700 ppm). As a result, Mn/Sr ratios are generally below 0.01 (fig. S6). This is strong evidence for the preservation of seawater geochemical signatures. Oxygen isotope values are > −7 ‰, which also suggests the lack of substantial meteoric or deep burial diagenesis.

In the Baimatuo Member, dolostone is characterized by relatively low Mn contents (< 150 ppm with the exception of three samples) and relatively low Sr concentrations (< 65 ppm) (fig. S6). Sr is easily expelled from the crystal lattice during recrystallization and dolomite has a generally lower preference for Sr than calcite, such that early fabric-retentive dolomite formed in the presence of seawater is often depleted in Sr. The low Mn contents and generally low Mn/Sr ratios of these samples (< 2.5 with the exception of six samples that have been excluded) indicate a high degree of preservation of seawater geochemistry, despite these low Sr contents. This hypothesis is also supported by oxygen isotope data ($\delta^{18}O$ values > −6 ‰). In summary, petrography and geochemistry both indicate that limestone and dolostone of the Shibantan and Baimatuo members are either primary precipitates or formed during early seafloor diagenesis.

In the Yanjiahe Formation, we excluded three samples based on high Mn contents, low Sr contents, and therefore, high Mn/Sr ratios (two samples with Mn/Sr > 15). The remaining samples are characterized by Mn contents < 100 ppm, Sr contents > 250 ppm, and oxygen isotope values > −7.5 ‰, suggesting preservation of seawater geochemistry (fig. S6).

In addition to absolute Mn and Sr contents, we have also investigated Mn/(Mg+Ca) and Sr/(Mg+Ca) ratios (fig. S7). Mn/(Mg+Ca) data strongly mirror the previously-discussed Mn contents, and suggest that no anomalous Mn enrichment occurred in the Wuhe section that can be attributed to late-stage diagenesis. In the Gaojiashan section, there is a trend of decreasing Mn/(Mg+Ca) upward in the section (fig. S7D). If this were caused by late-stage burial diagenesis or pore water anoxia during early diagenesis, then we would also expect systematic differences in $\delta^{238}U$, with higher $\delta^{238}U$ in the lower interval compared to the upper interval. This is not observed, however, suggesting that $\delta^{238}U$

values were not systematically altered by early pore water anoxia or late-stage burial diagenesis. We also note that $\delta^{238}U$ in the Gaojiashan section is identical to the well-preserved, coeval Shibantan Member at the Wuhe section, suggesting that both sections record primary values. Sr/(Mg+Ca) values also mirror the previously-discussed Sr contents, and show expected trends related to carbonate mineralogy.

In the Wuhe section as a whole, there is no correlation between carbon and oxygen isotope values ($R^2 = 0.009$; fig. S8). $\delta^{13}C$ and $\delta^{18}O$ tend to co-vary if both systems have been influenced by proportional mixing with an external (diagenetic) fluid, and in the case of the Wuhe section, the lack of co-variation between these parameters is another line of evidence supporting preservation of early, seawater-derived geochemical signatures.

Lastly, in the Gaojiashan section, the lower 30 meters are characterized by Mn > 300 ppm (with the exception of one sample), Sr < 150 ppm (with the exception of two samples), and highly variable oxygen isotope values ranging from −1.78 to −8.39 ‰ (fig. S6). Mn/Sr ratios are uniformly > 2.5, and we have therefore excluded eight samples from this interval. By contrast, the upper part of the section is characterized by low Mn contents (< 300 ppm with the exception of one sample), relatively high Sr contents (most samples > 400 ppm), low Mn/Sr ratios (< 1.5), and oxygen isotope values > −7.5 ‰ (with the exception of one sample). There is also no co-variation between carbon and oxygen isotopes for the entire Gaojiashan section ($R^2 = 0.017$; fig. S8), which would be expected if both parameters were influenced by proportional mixing with an external fluid. These data, along with generally fabric-retentive petrographic characteristics, strongly indicate that the upper 20 meters of the Gaojiashan section have the potential to record seawater geochemistry.

Using these diagenetic criteria, 2, 0, 6, and 2 outliers have been identified from the Hamajing Member (total sample number #8), the Shibantan Member (total sample number #24), the Baimatuo Member (total sample number #23), and the Yanjiahe Formation (total sample number #7) at the Wuhe section. Eight outliers have been identified from the Gaojiashan Member (total sample number #27) at the Gaojiashan section.

Because the main conclusions of our study are based on the very light U isotope compositions recorded in the Shibantan and Gaojiashan members, we further investigated the extent of correlation between $\delta^{238}U$ and $\delta^{18}O$, Sr concentration, Mn concentration, and Mn/Sr for samples in these units with Mn/Sr ratios < 2.5 (table S2). There is no systematic correlation between diagenetic indicators and $\delta^{238}U$ in the Shibantan and Gaojiashan members, suggesting that late-stage diagenesis did not progressively alter U isotope values. It is also important to note that these very light U isotope values are found in two geographically disparate, but coeval sections, which also argues against systematic alteration of U isotopes.

Detrital contaminations

When evaluating detrital contamination, we used detrital indicators such as Rb/Sr ratios and Al contents (e.g., Ling *et al*. (*40*)). Among samples with Mn/Sr < 2.5, only those samples with Rb/Sr < 0.02 and Al (wt.%) < 0.35 % were used in our main text discussion. The Rb/Sr and Al content plots are shown in fig. S9.

In addition, for samples with Mn/Sr < 2.5, Rb/Sr < 0.02 and Al < 0.35%, we further looked at U/Al ratios to confirm that our dissolution procedure primarily targets carbonate-bound (and not detrital) U. The U/Al ratio of the upper continental crust is ~0.331 ppm/wt.% (*85*), and U/Al ratios in our samples are substantially enriched above crustal values by approximately two orders of magnitude (fig. S9), indicating that the dissolution procedure is effective at isolating carbonate-bound U.

We have also used Al content (wt.%) data to estimate the possible amount of contribution of U from detrital sources. Specifically, assuming all the measured Al in our samples is from detrital minerals, and using the U/Al ratio of upper continental crust, we estimate that detrital U accounts for <2 % of total U for Wuhe samples, and < 10 % of total U for Gaojiashan samples. Thus, we conclude that detrital influence on our δ^{238}U signals are minimal. We also note that the estimated amount of U associated with detrital material is different between the Shibantan Member at Wuhe and its equivalent Gaojiashan Member. However, the δ238U signals of these two members are identical.

Ce anomalies and dolomitization

Romaniello *et al*. (*29*) point out that in the modern Bahamas, bulk carbonate sediments can incorporate U with a δ^{238}U value that is 0.2–0.4 ‰ heavier than seawater due to the incorporation of ^{238}U-enriched U(IV) under locally pore water euxinic conditions. If this were true in our Dengying carbonates, then we could have potentially underestimated the extent of U removal associated with anoxic sedimentary sinks.

First, we examined local water column redox conditions by looking at the Ce anomaly (Ce/Ce*) recorded in our carbonate samples. Unlike the other REEs, which are strictly trivalent in the oceans, cerium (Ce) can exist in either trivalent or tetravalent forms depending on redox conditions. The redox state of Ce is modulated by the presence of manganese oxides and/or bacteria, where Ce is oxidized by and adsorbed onto mineral surfaces (*40*). Thus, the concentration of Ce relative to the other REEs is associated with dissolved oxygen concentrations, and can be used to infer redox conditions of the overlying water column (*20, 40*).

Ce anomalies are calculated following Ling *et al*. (*40*). The Ce anomalies at Wuhe range between 0.29 and 0.79 with a mean of 0.5, and the Ce anomalies at Gaojiashan range between 0.70 and 0.98 with a mean of 0.76 (fig. S10). The Ce anomalies indicate that the local water column at both Wuhe and Gaojiashan were likely dominated by oxic conditions (*40, 86*). This confirms that our carbonates can be considered an oxic sink for U, and thus can passively capture the δ^{238}U signal of seawater.

Second, we examined the possibility of pore water euxinia using Mo and U concentrations, as well as correlations between $\delta^{238}U$ and U/(Mg+Ca) ratios and Mo/(Mg+Ca) ratios (fig. S10). Under euxinic pore water conditions, U and Mo become authigenically enriched in carbonate (*29, 87*), thus increasing [Mo], [U], U/(Mg+Ca), and Mo/(Mg+Ca) values. In our samples from both sections, Mo concentrations are <0.2 ppm, with the exception of two samples (BM-1 and YJH-40). This is in contrast to carbonate sediments from the modern Bahamas, most of which are characterized by Mo concentrations between 1.8 and 28 ppm (*87*). This indicates that pore water euxinia was less prevalent during deposition of our samples than on the modern Bahamian carbonate platform. In addition, U/(Mg+Ca) and Mo/(Mg+Ca) are extremely low (excluding two samples, BM-1 and YJH-40) and there is no systematic stratigraphic variation. Furthermore, there are no statistically significant correlations between $\delta^{238}U$ and U/(Mg+Ca) and Mo/(Mg+Ca) in our carbonates (table S2). We note that although the two "outliers", the BM-1 and the YJH-40, were likely affected by pore water anoxia during early diagenesis, their $\delta^{238}U$ did not depart from the surrounding samples with low U concentrations. If there were U addition (compared to the surrounding low U concentration samples) associated with pore water anoxia during early diagenesis, that would indicate 60–100% of U in these two samples are related to proewater anoxia, and thus these samples would show obvious high $\delta^{238}U$ values. However, this is in contrast to our observations that $\delta^{238}U$ of these three samples did not obviously depart from the surrounding low U concentration samples. And thus, these high concentrations might have been caused by other factors that did not affect $\delta^{238}U$.

Romaniello *et al*. (*29*) also observed U-isotope change associated with dolomitization in one Bahamian tidal pond. There was a strong correlation with Mg/Ca ratio (R^2=0.96), suggesting that U-isotope change was possibly associated with dolomitization. This seems to be a special, spatially restricted case, however. In our samples from Wuhe, no statistically significant correlations are observed between $\delta^{238}U$ and Mg/Ca molar ratio (R^2=0.25), suggesting that dolomitization has not systematically altered the primary isotopic record. Further confidence that dolomitization may not have been an issue for paleo-$\delta^{238}U$ records comes from a global compilation of $\delta^{238}U$ studies across the Permian-Triassic boundary. Both the dolomitized section (the Dawen section in South China; Brennecka *et al*. (*19*)) and the non-dolomitized sections (the Kamura section in Japan, the Dajiang section and the Daxiakou section in South China, and the Taskent section in Turkey; Lau *et al*. (*88*); Elrick *et al*. (*89*); Zhang *et al*. (*21*)) show congruent $\delta^{238}U$ records. Despite potential uncertainty regarding dolomitization, the bulk of our conclusions hinge on the very light $\delta^{238}U$ values observed in limestone of the Shibantan and Gaojiashan members. Both of our limestone sections (Wuhe and Gaojiashan) record these very light values, and we consider these results to be robust regardless of dolomitization in the underlying Hamajing Member and the overlying Baimatuo Member.

Uranium isotope mass balance constraints on U removal to anoxic/euxinic sinks

The implied changes to the extent of U removal into anoxic sediments can be described by a mass balance equation for the fraction of anoxic/euxinic sinks and their isotopic composition (following Montoya-Pino *et al*., (*90*))

$$\delta^{238}U_{input} = (f_{anoxic} \times \delta^{238}U_{anoxic}) + (f_{other} \times \delta^{238}U_{other}) \qquad (1)$$

$$\delta^{238}U_{anoxic} = \delta^{238}U_{seawater} + \Delta_{anoxic} \qquad (2)$$

$$\delta^{238}U_{other} = \delta^{238}U_{seawater} + \Delta_{other} \qquad (3)$$

$$f_{anoxic} + f_{other} = 1 \qquad (4)$$

Solving equations (1) to (4), we have

$$f_{anoxic} = (\delta^{238}U_{input} - \delta^{238}U_{seawater} - \Delta_{other})/(\Delta_{anoxic} - \Delta_{other}) \qquad (5)$$

Here, the subscripts input, anoxic, and other denote the riverine input, anoxic/euxinic sink, and other sedimentary sinks, respectively, and f_{anoxic} represents the fraction of the riverine U input that is deposited in anoxic/euxinic sediments. Following Montoya-Pino et al. (90) and Brennecka et al. (19), we assume: (1) isotopically constant U input from rivers over geologic time with an average value of −0.34 ‰ (59) ($\delta^{238}U_{input}$ = −0.34 ‰); (2) a constant isotope fractionation between seawater and the average isotopic composition of other sinks, including suboxic sinks, ferromanganese oxides, and hydrothermal alteration of oceanic crust (Δ_{other} = +0.043 ‰) (fig. S1); and (3) a fractionation factor of Δ_{anoxic} between seawater and anoxic/euxinic sinks between 0.4 ‰ and 1.2 ‰. Based on the assumptions above and our measured U isotope values from the Dengying Formation ($\delta^{238}U_{Ediacaran\ seawater}$ = −0.95 ‰, $\delta^{238}U_{input}$ = −0.34 ‰, $\delta^{238}U_{other\ sinks}$ = −0.907 ‰ (i.e., −0.95 + 0.043 ‰), and $\delta^{238}U_{anoxic\ sinks}$ = −0.95 ‰ + Δ_{anoxic}), we can derive a function for f_{anoxic} that depends on Δ_{anoxic}: f_{anoxic} = 0.567 / (Δ_{anoxic} − 0.043).

The estimated f_{anoxic} values can change with the $\delta^{238}U_{input}$ values used in the calculation. The present study used the global average riverine value reported by Andersen et al. (59). Another study by Noordmann et al. (60) have reported a slightly lighter average riverine value of −0.27 ‰ (all major rivers define a relatively narrow range between −0.31 and −0.13 ‰ with a weighted mean isotope composition of −0.27 ‰). However, the difference in average riverine values will only result in small differences in the estimated f_{anoxic} values. For instance, when applying a Δ_{anoxic} of 0.835 ‰ (discussed below), f_{anoxic} = (0.907 + $\delta^{238}U_{input}$) / 0.792, when using $\delta^{238}U_{input}$ of −0.34 ‰, −0.27 ‰, and −0.20 ‰, the estimated f_{anoxic} are 72%, 80%, and 89%, respectively.

Anoxic seafloor area modeling calculation

The fraction of U removed into anoxic/euxinic sediments can be coupled to the extent of seafloor covered by anoxic/euxinic waters, as described by Wang et al. (55), Lau et al. (88), and Zhang et al. (28) and shown in Fig. 3B of the main text and fig. S11 of the Supplementary Information. Below is a summary of the modeling method:

The implied changes to the extent of bottom water anoxia can be described by differential mass balance equations for the seawater uranium inventory and its isotopic composition, respectively (following Wang *et al.* (*55*), Lau *et al.* (*88*), and Zhang *et al.* (*28*))

$$\frac{dN_{sw}}{dt} = J_{riv} - J_{oxic} - J_{anoxic} - J_{suboxic}$$
(6)

$$\frac{d(N_{sw} \times \delta^{238}U)}{dt} = J_{riv} \times \delta^{238}U_{riv} - J_{oxic} \times \delta^{238}U_{oxic} - J_{anoxic} \times \delta^{238}U_{anoxic} - J_{suboxic} \times \delta^{238}U_{suboxic}$$
(7)

$$\delta^{238}U_{oxic} = \delta^{238}U_{sw} + \mathrm{D}_{oxic}$$
(8)

$$\delta^{238}U_{anoxic} = \delta^{238}U_{sw} + \mathrm{D}_{anoxic}$$
(9)

$$\delta^{238}U_{suboxic} = \delta^{238}U_{suboxic} + \mathrm{D}_{suboxic}$$
(10)

$\delta^{238}U_{sw}$ and $\delta^{238}U_{riv}$ are the U isotope composition of seawater and the riverine source, respectively. $\delta^{238}U_{anoxic}$, $\delta^{238}U_{suboxic}$, and $\delta^{238}U_{oxic}$ are the U isotope composition of anoxic sedimentary sink, suboxic sedimentary sink, and the sum of the other sinks, respectively. Here, we simplify the inputs to J_{riv}, the riverine flux, whose modern value is ~4×10⁷ moles U/yr (*54*). The outputs are assumed to consist of the anoxic sediment sink (J_{anoxic}), suboxic sediment sink ($J_{suboxic}$), and the sum of the other sinks (J_{oxic}). Δ_{anoxic} is the effective fractionation factor associated with anoxic sediment deposition, $\Delta_{suboxic}$ is the effective fractionation factor associated with suboxic sediment deposition, and Δ_{oxic} is the effective fractionation factor associated with the remaining other sinks (+0.005‰, calculated to maintain isotopic steady state in the modern ocean (e.g, Brennecka *et al.* (*19*), Montoya-Pino *et al.* (*90*), and Wang *et al.* (*55*)).

At steady state, the left side of the equation (6) and (7) equal 0, yielding

$$J_{riv} = J_{oxic} + J_{anoxic} + J_{suboxic}$$
(11)

$$J_{riv} \times \delta^{238}U_{riv} = J_{oxic} \times \delta^{238}U_{oxic} + J_{anoxic} \times \delta^{238}U_{anoxic} + J_{suboxic} \times \delta^{238}U_{suboxic}$$
(12)

We define the oxic, anoxic, and suboxic sinks in Eq. 6–12 assuming a first-order dependence on seawater U concentration (*88, 91, 92*)

$$J_{oxic} = k_{oxic} \times N_{sw} \times A_{oxic}$$
(13)

$$J_{anoxic} = k_{anoxic} \times N_{sw} \times A_{anoxic}$$
(14)

$$J_{suboxic} = k_{suboxic} \times N_{sw} \times A_{suboxic} \tag{15}$$

where A_{oxic}, A_{anoxic}, and $A_{suboxic}$ are the total seafloor area overlain by oxic waters, anoxic waters, and suboxic waters, respectively. k_{oxic} k_{anoxic}, and $k_{suboxic}$ are rate constants associated with oxic sediment deposition, anoxic sediment deposition, and suboxic sediment deposition and are calculated for the modern uranium system (e.g., Wang *et al.* (*55*), Lau *et al.* (*88*), and Zhang *et al.* (*28*)).

We further define the fraction of anoxic seafloor area overlain by anoxic water

$$F_{anoxic} = \frac{A_{anoxic}}{A_{ocean}} \tag{16}$$

where F_{anox} is the total fraction of seafloor area overlain by anoxic waters, and A_{ocean} is the total seafloor area of modern ocean. Model parameterization was based on studies of the modern U cycle and are summarized in table S3. Modeling results are summarized in Fig. 3B of the main text and fig. S11 of the Supplementary Information.

Solving equations 6–15, we have

$$\delta^{238}U_{sw} = \delta^{238}U_{riv} - \frac{A_{anoxic} \cdot k_{anoxic} \cdot D_{anoxic} + A_{suboxic} \cdot k_{suboxic} \cdot D_{suboxic} + A_{oxic} \cdot k_{oxic} \cdot D_{oxic}}{A_{anoxic} \cdot k_{anoxic} + A_{suboxic} \cdot k_{suboxic} + A_{oxic} \cdot k_{oxic}} \tag{17}$$

where $A_{anoxic} + A_{suboxic} + A_{oxic} = A_{ocean}$.

In this modeling, we adopted a value of −0.34‰ for rivers. As stated earlier, riverine input is the single major source of U into the ocean. The weighted average $\delta^{238}U$ of riverine input is −0.34 ‰ (*59*). An exception not included in this average is the Yangtze River in China, where two reported measurements yield an average $\delta^{238}U$ value of ~−0.70 ‰. Although these data and their ability to represent the entire Yangtze catchment need to be confirmed, this "outlier" is interpreted to reflect local U contributions from evaporite minerals (halite) that are abundant near the source of the Yangtze River. If so, this is an unusual situation because evaporites are not major sources of U to the oceans overall. Previous global riverine estimates yielded values of −0.30 ‰ to −0.27 ‰ (*60*). It thus appears that the riverine composition is indistinguishable from average continental crust, which has been measured as −0.30 ± 0.04 ‰ and −0.31 ± 0.05 ‰ (*60*).

In this modeling exercise, we have simplified the ocean into oxic, suboxic, and anoxic states. Because of the fractionation factor of U isotopes under suboxic conditions are from $\delta^{238}U$ measurements from the Peruvian continental margin (*23*) and off the coast of Washington State (*59*), and hence, by referring to suboxic conditions, we are discussing a situation that is similar to suboxic waters in Peruvian continental margin and off the coast of Washington State. Bottom water O_2 at both Peruvian continental margin and off the coast of Washington State are within the range of 0.2 to 2 ml L^{-1} that has previously been

used to define suboxic depositional environments (*93*). Similarly, the fractionation factor of U isotopes under anoxic conditions are primarily based on observations from the modern Black Sea and from the modern Saanich Inlet, and therefore, by referring to anoxic conditions, we are discussing a situation that is similar to these two modern anoxic environments. Here, bottom water O_2 concentrations are <0.2 ml L^{-1} and H_2S concentrations >400 μM (*42*).

We first varied the areal extent of anoxic/euxinic and oxic seafloor area while keeping the areal extent of suboxic seafloor the same as the modern value [$f_{suboxic}$=6%, black curve in fig. S11]. This modeling exercise suggests that essentially the entire seafloor was covered by anoxic/euxinic sediments (assuming a fractionation factor of 0.6 ‰ between seawater and anoxic/euxinic sediments) for terminal Ediacaran seawater $\delta^{238}U$ to approach values as low as −0.95 ‰. In reality, however, suboxic seafloor area is likely to co-vary with anoxic/euxinic seafloor area. We tested various suboxic areal extents [0 %, 6 %, 20 %, 30 %, 40 %, 50 %, and 75 %; fig. S11], the results of which tell us that it is difficult or even impossible to generate seawater $\delta^{238}U$ of −0.95 ‰ with large suboxic seafloor areas (assuming anoxic/euxinic sink-seawater fractionation of 0.6 ‰). Thus, variations in suboxic seafloor area have a very small effect on our basic conclusion that significantly expanded anoxic/euxinic seafloor area is likely the only major process that can cause terminal Ediacaran seawater $\delta^{238}U$ to reach values as low as −0.95 ‰.

Second, we varied the fractionation factor between seawater and anoxic/euxinic sediments and kept the suboxic seafloor area fixed at 0%. These results are summarized in Fig. 3B in the main text. Our results suggest that the inferred extent of ocean anoxia largely depends on the assumed average fractionation factor between seawater and anoxic/euxinic sediments. If we use larger fractionation factors of 0.68 ‰ and 0.99 ‰— the two end member values observed for reduction of U(VI) to U(IV) by metal-reducing bacteria (*27*)—modeling results suggest that ~33 % and ~8.5 % of anoxic/euxinic seafloor area was required to drive terminal Ediacaran seawater $\delta^{238}U$ to values as low as −0.95 ‰.

We also ran our model with a Δ_{anoxic} of 0.835 ‰, which is an "average" fractionation factor that represents microbially-mediated U reduction (*27*), and is close to the maximum Δ_{anoxic} observed both in the modern Saanich Inlet (0.79 ‰) (*41*) and in the Black Sea (0.83 ‰) (*23*). Here, we calculate that f_{anoxic} = 0.7, meaning that a minimum of 70 % of global riverine U input was removed into anoxic/euxinic sediments when the Shibantan/Gaojiashan members were deposited. This fraction of U removal into anoxic/euxinic sediments is estimated to occur over an anoxic/euxinic seafloor area of ~14 %. In reality, suboxic seafloor area would not be 0 % and would co-vary with expanded anoxic/euxinic seafloor area. If we assume that $f_{suboxic}$ was greater than f_{anoxic} in the latest Ediacaran ocean, then a combination of $f_{suboxic}$ = 21% and f_{anoxic} = 21% will minimally be required in order to account for latest Ediacaran seawater average $\delta^{238}U$ of −0.95‰ (fig. S12). In reality, 21% seafloor area overlain by anoxic waters will require an even larger seafloor area overlain by suboxic seafloor area. For example, the f_{anoxic} = ~0.35% while $f_{suboxic}$ = 6% in the modern ocean. We therefore conclude that at least 42%

of the seafloor was covered by oxygen-deficient (anoxic + suboxic) waters. However, in the abstract of the main text, we focus on emphasizing anoxic seafloor areas.
This simple modeling exercise thus gives us the lowest estimate of anoxic/euxinic seafloor area. Parameters used in the modeling exercise have been summarized in table S3.
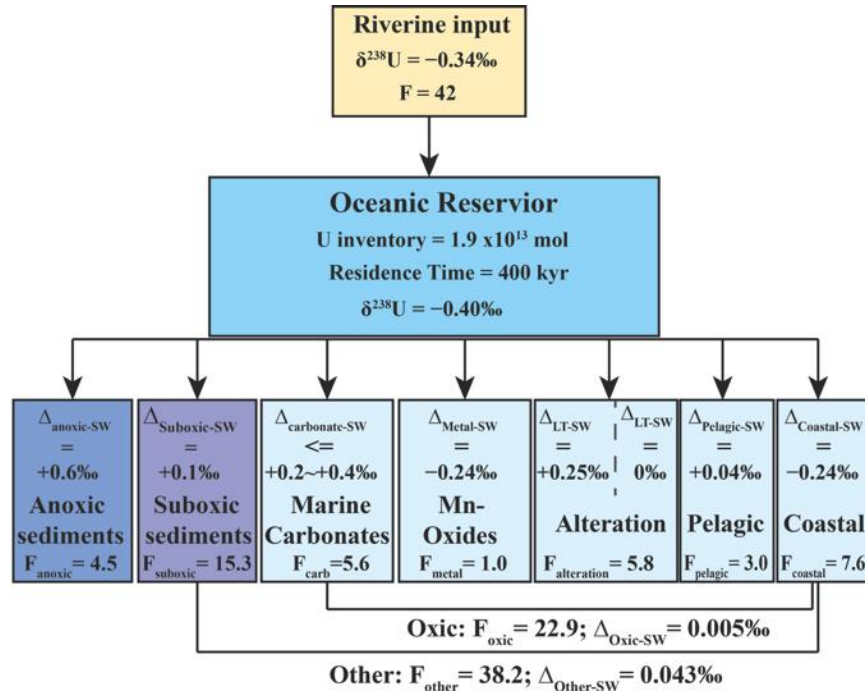
Supplementary figures

fig. S1. Simplified schematic representation of the major source and sinks of U in the modern ocean along with their isotopic compositions (sources) or associated isotopic fractionations (sinks) [modified after Tissot and Dauphas (*54*) and Wang *et al.* (*55*)]. The $\delta^{238}U$ of riverine input was from Andersen *et al.* (*59*). In the alteration box, LT denotes low temperature alteration, and HT denotes high temperature alteration. Sinks including suboxic, carbonates, Mn-oxides, oceanic crust alteration, pelagic clays, and coastal retention are treated as one single "other" sink, with the fractionation factors being the weighted average of these individual sinks. All flux data (F) have a unit of 10^6 mol/yr.
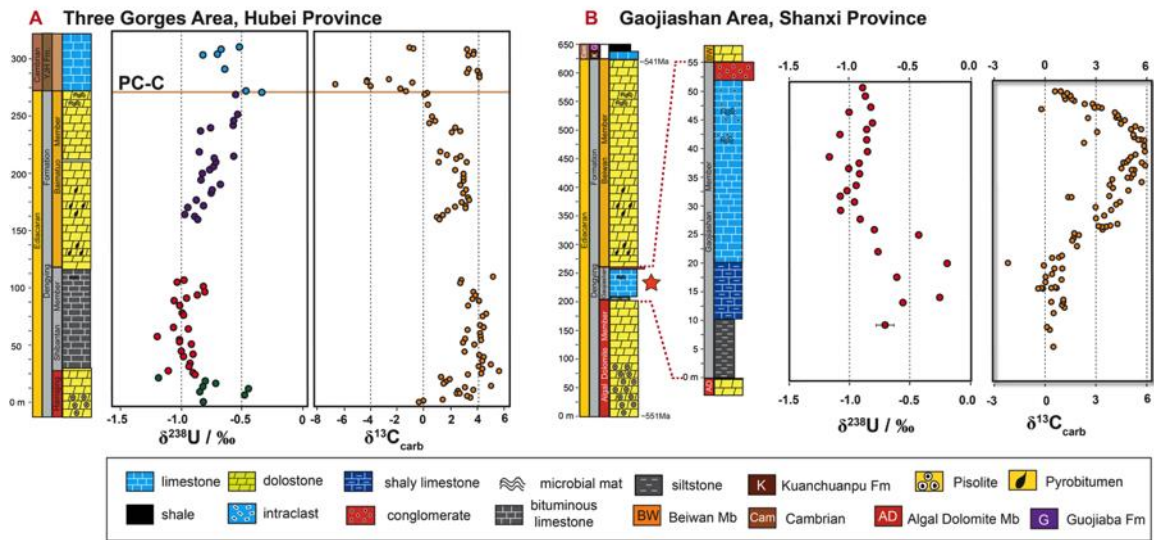
fig. S2. Geochemical profiles for the study sections. Geochemical profiles of (**A**) the Dengying Formation and Yanjiahe Formation from the Wehe section, and (**B**) the Gaojiashan member from the Gaojiashan section. δ^{13}C data of the Gaojiashan member are from Cui *et al.* (*31*).
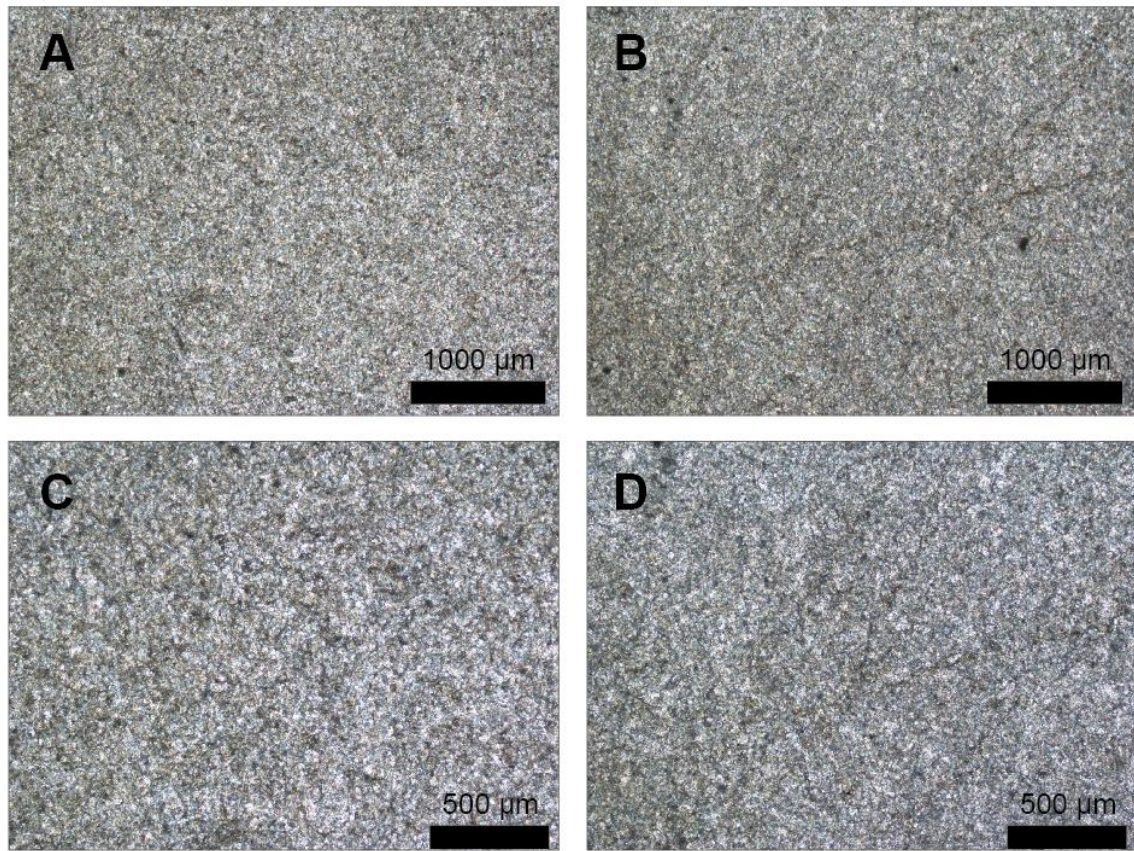
fig. S3. Petrographic images of the Hamajing Member. Petrographic photos from the Hamajing dolomite (**A** to **D**) at the Wuhe section. Photos are of samples HMJ-14 (A, C) and HMJ-19 (B, D).
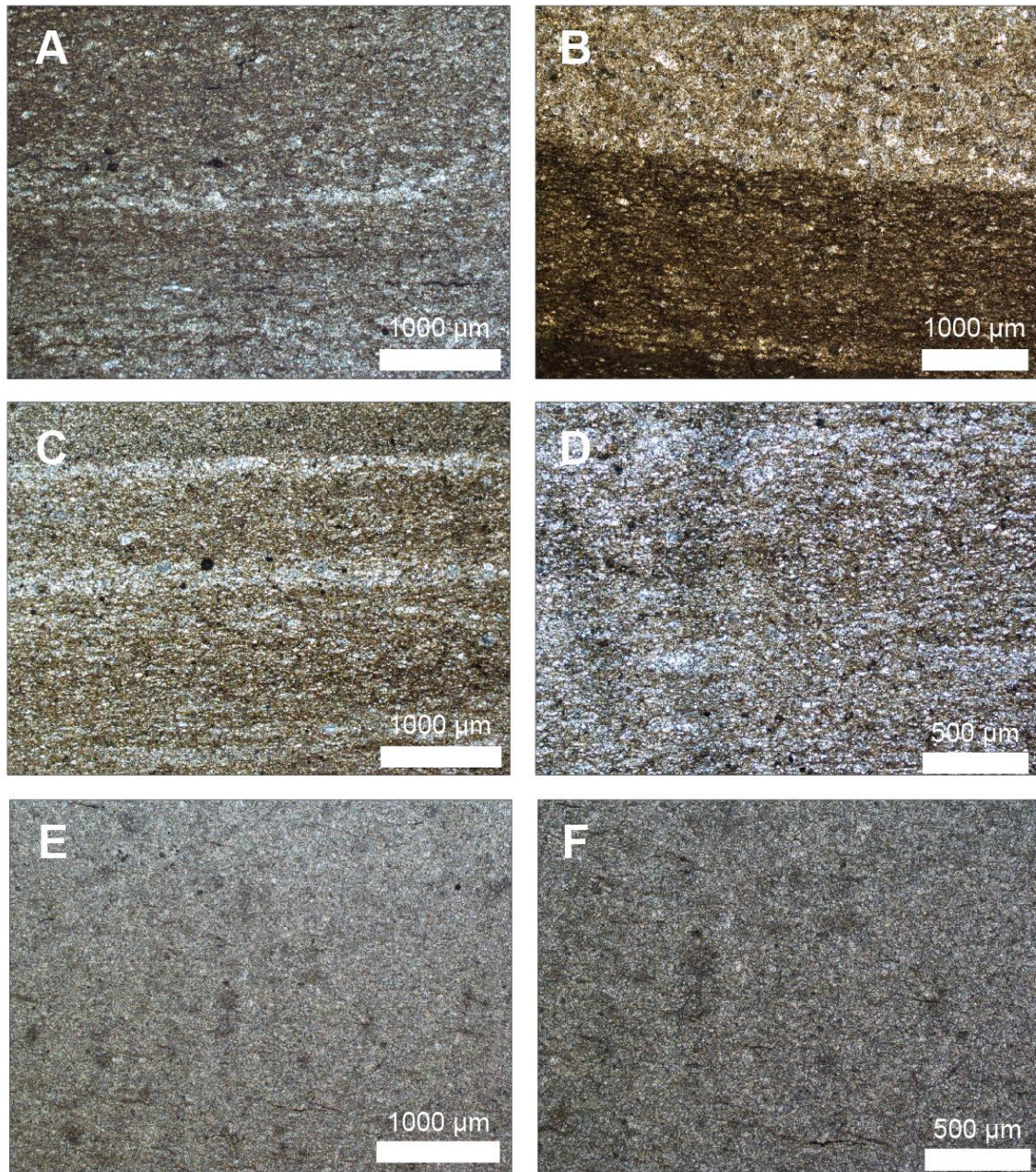
fig. S4. Petrographic images of the Shibantan Member. Petrographic photos from the Shibantan limestone (**A** to **F**) at the Wuhe section. Photos are of sample SBT-89 (A), SBT-26 (B), SBT-42 (C, D), and SBT-107 (E, F).
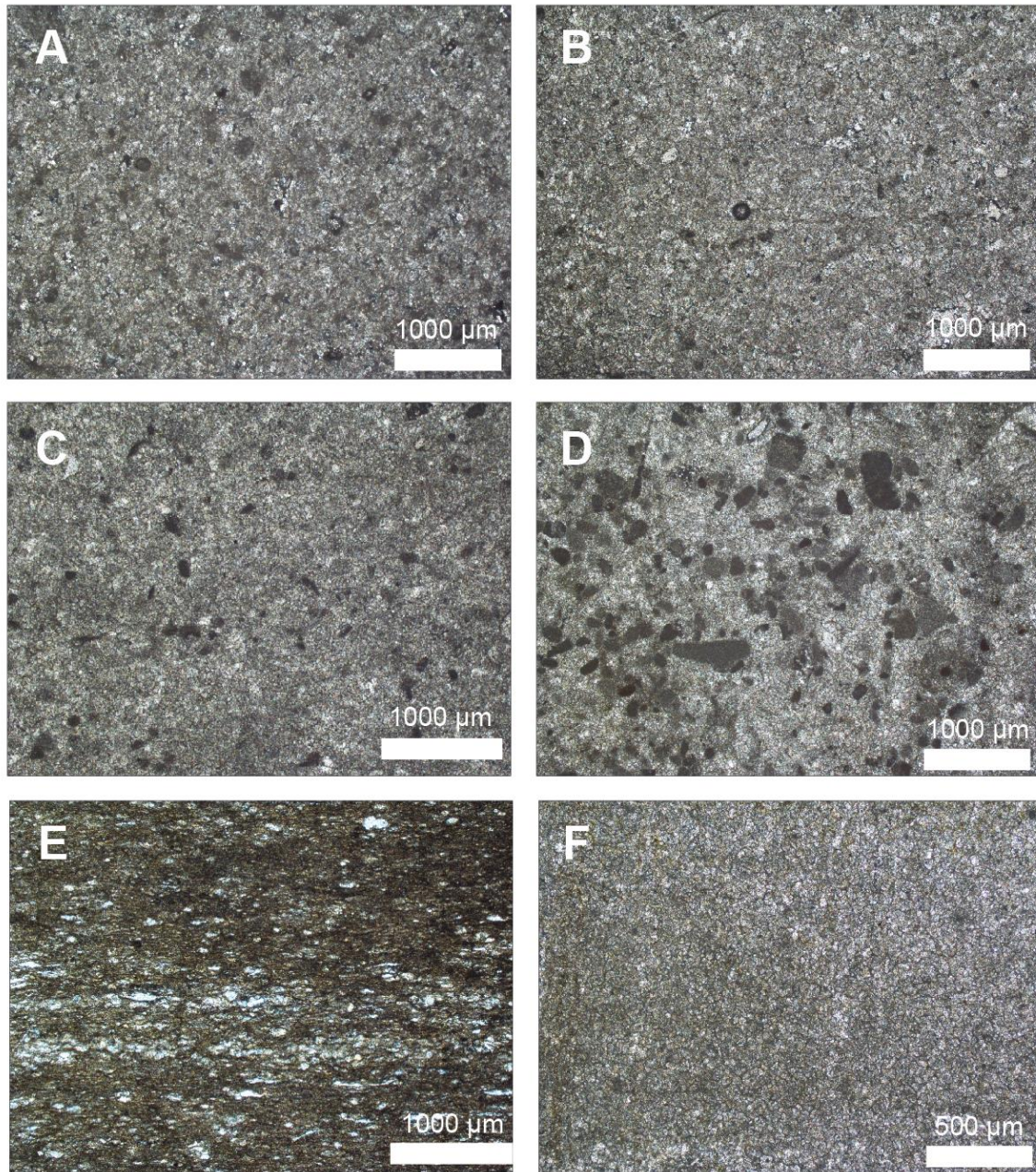
fig. S5. Petrographic images of the Baimatuo Member and the Yanjiahe Formation. Petrographic photos from the Baimatuo dolomite (**A** to **C**) and the Yanjiahe limestone (**D** to **F**) at the Wuhe section. Photos are of sample BMT-172 (A), BMT-186 (B), BMT-200 (C), YJH-2 (D), YJH-21 (E), and YJH-30 (F).
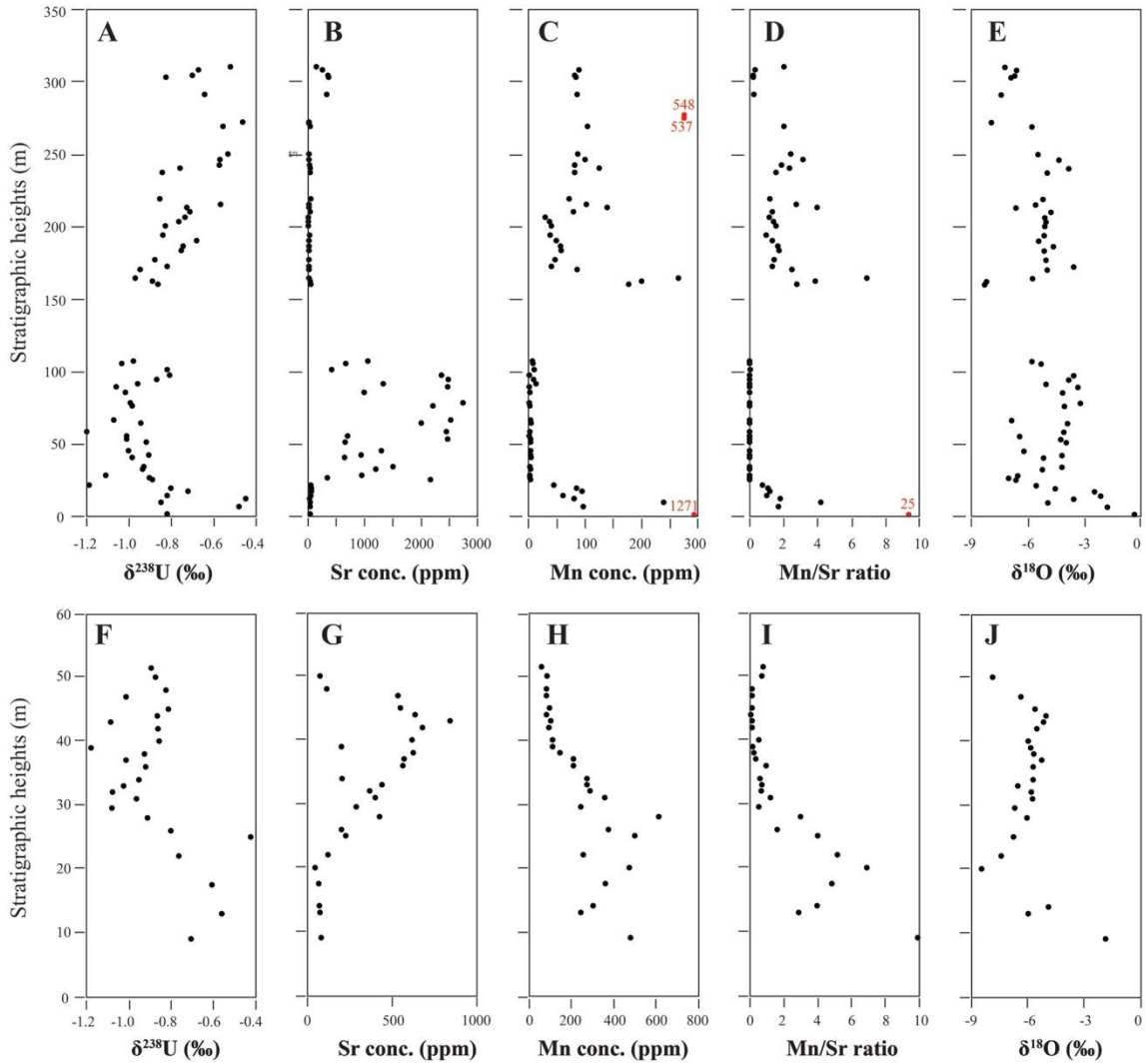
fig. S6. Chemostratigraphic profiles of δ²³⁸U, Sr content, Mn content, Mn/Sr ratio, and δ¹⁸O for the study sections. δ^{238}U, Sr concentration, Mn concentrations, Mn/Sr ratios, and δ^{18}O profiles for samples from Wuhe (**A** to **E**) and Gaojiashan (**F** to **J**).
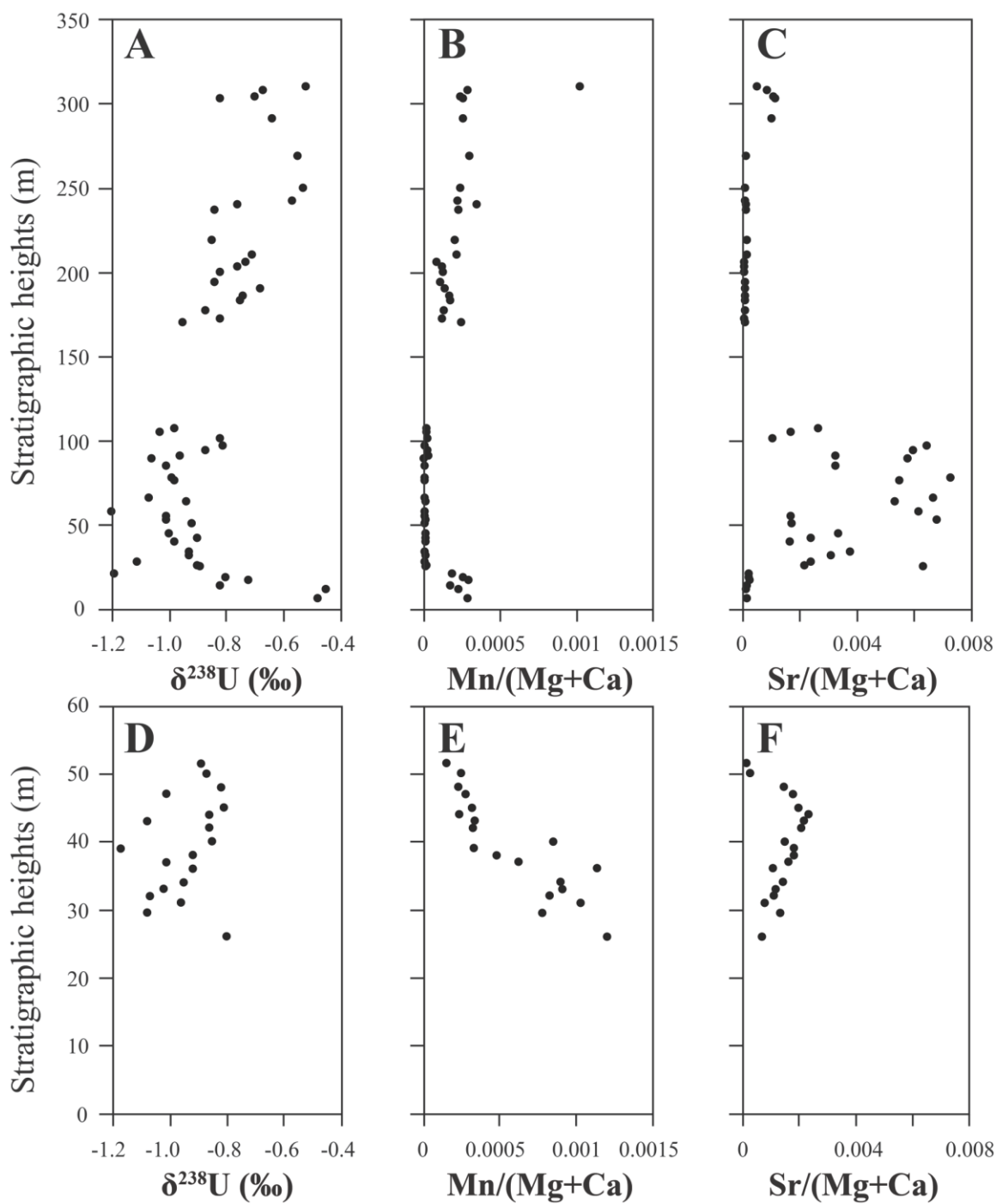
fig. S7. Chemostratigraphic profiles of δ²³⁸U, Mn/(Mg + Ca) ratio, and Sr/(Mg + Ca) ratio for the study sections. δ^{238}U, Mn/(Mg+Ca) ratio, and Sr/(Mg+Ca) ratio profiles for samples from Wuhe (**A** to **C**) and Gaojiashan (**D** to **F**).
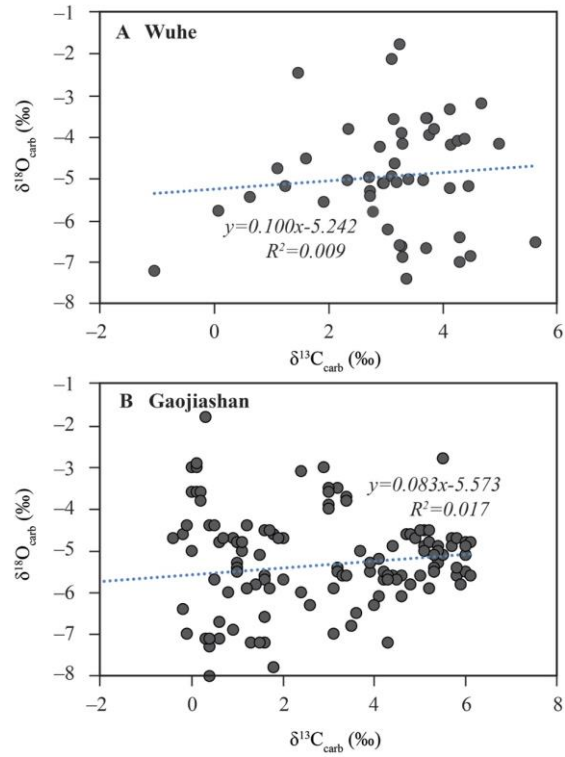
fig. S8. Cross-plots of δ¹³C-δ¹⁸O for the study sections. $\delta^{13}C$ and $\delta^{18}O$ correlations of the Wuhe section (**A**) and the Gaojiashan section (**B**). No systematically significant correlations have been observed for both sections.
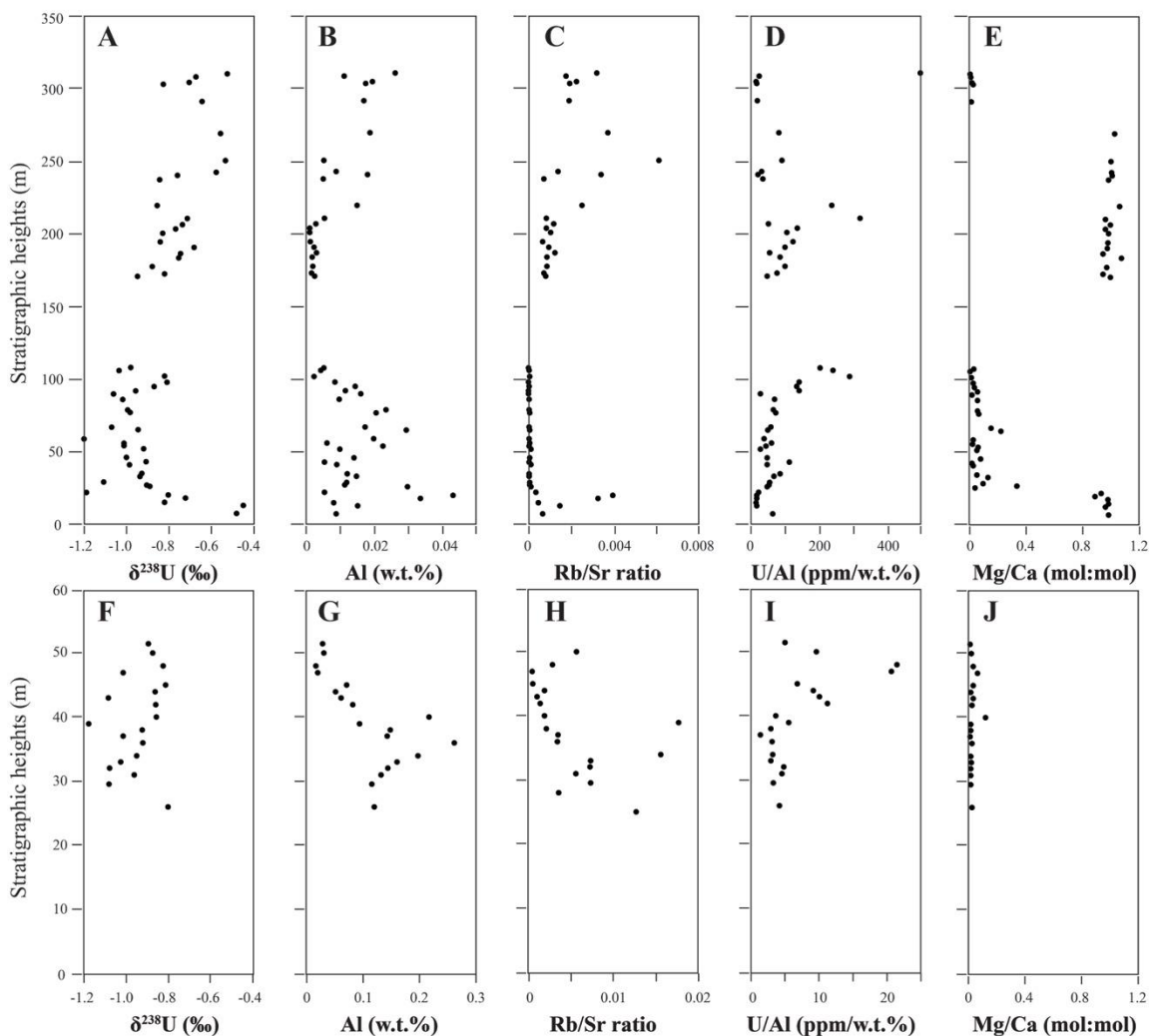
fig. S9. Chemostratigraphic profiles of δ²³⁸U, Al content, Rb/Sr ratio, U/Al ratio, and Mg/Ca molar ratio for the study sections. δ^{238}U, Al content (w.t.%), Rb/Sr ratios, U/Al ratios (ppm/w.t.%), and Mg/Ca ratio (mol:mol) profiles for samples from Wuhe (**A** to **E**) and Gaojiashan (**F** to **J**). Samples with Mn/Sr>2.5 have been excluded from these plots.
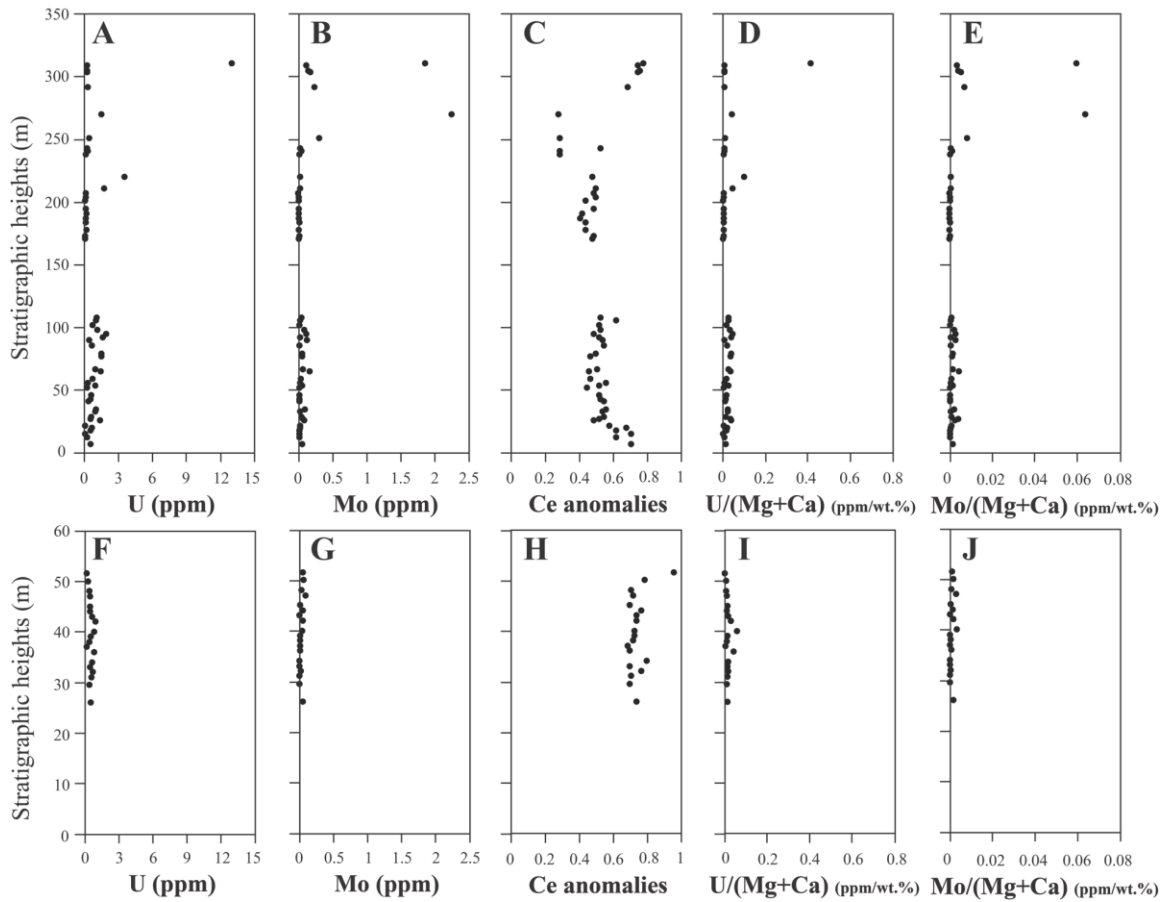
fig. S10. Chemostratigraphic profiles of U and Mo concentrations, Ce anomalies, U/(Mg + Ca) ratio, and Mo/(Mg + Ca) ratio for the study sections. U concentration, Mo concentrations, calculated Ce anomalies, U/(Mg+Ca) ratio, and Mo/(Mg+Ca) ratio profiles for samples from Wuhe (**A** to **E**) and Gaojiashan (**F** to **J**). Samples with Mn/Sr>2.5 have been excluded from these plots.
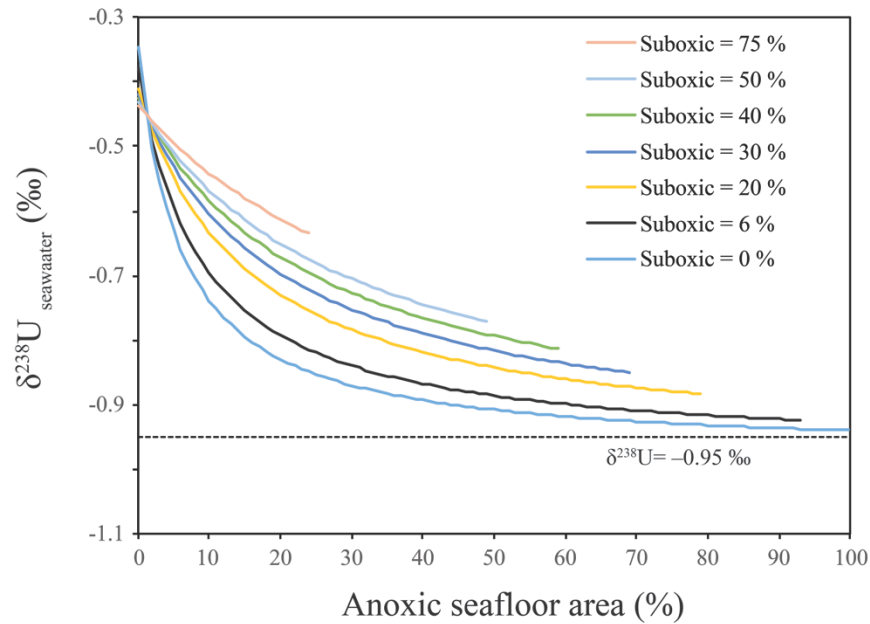
fig. S11. Mass balance modeling calculations show variations of seawater δ²³⁸U values as a function of anoxic/euxinic seafloor area while keeping Δ$_{anoxic}$ constant (+0.6‰) and testing various suboxic areal extents.

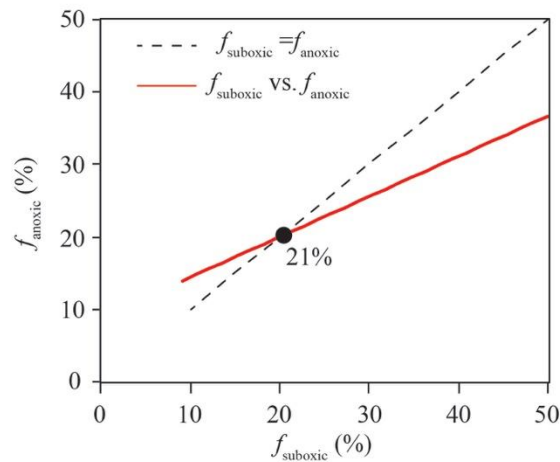**fig. S12. Calculated combination f_{anoxic} and $f_{suboxic}$ to account for latest Ediacaran seawater average δ²³⁸U of −0.95‰.** The black dash line is a reference where equals f_{anoxic} to $f_{suboxic}$. The red solid line denotes a combination f_{anoxic} and $f_{suboxic}$ in order to account for latest Ediacaran seawater average δ²³⁸U of -0.95‰.

Supplementary tables

table S1. The sample-dissolving procedure.

Dissolving step	Dissolving agent	Time gap between steps
S1–S6	5mL 1M HCl	10 minutes
S7–S11	1mL 12M HCl	25 minutes
S11–S13	5mL 1M HCl	10 minutes
Final volume	45 mL	

S denotes steps, for instance, S1–S6 denote steps 1 to 6.

table S2. Cross-correlation coefficients (R^2) and P values calculated to test the influence of diagenetic indicators on $\delta^{238}U$ (confidence interval, 95%).

Shibantan Member at Wuhe	R^2	p-value
$\delta^{238}U$ vs. $\delta^{13}C$	0.21	0.33
$\delta^{238}U$ vs. Mg/Ca (mol:mol)	0.00	0.78
$\delta^{238}U$ vs. $\delta^{18}O$	0.02	0.53
$\delta^{238}U$ vs. Sr concentration	0.03	0.37
$\delta^{238}U$ vs. Mn concentration	0.08	0.17
$\delta^{238}U$ vs. Mn/Sr	0.12	0.09
$\delta^{238}U$ vs. Mn/(Mg+Ca) (ppm/w.t.%)	0.35	0.09
$\delta^{238}U$ vs. Sr/(Mg+Ca) (ppm/w.t.%)	0.15	0.50
$\delta^{238}U$ vs. Ce anomalies	0.01	0.65
$\delta^{238}U$ vs. U/Al (ppm/w.t.%)	0.15	0.06
$\delta^{238}U$ vs. Al content	0.19	0.38
$\delta^{238}U$ vs. U/(Mg+Ca) (ppm/ wt.%)	0.33	0.12
$\delta^{238}U$ vs. Mo/(Mg+Ca) (ppm/ wt.%)	0.22	0.31
$\delta^{238}U$ vs. Mo/U	0.00	1.00
$\delta^{238}U$ vs. Fe/U (wt.%/ppm)	0.06	0.24

Gaojiashan Member at Gaojiashan	R^2	p-value
$\delta^{238}U$ vs. $\delta^{13}C$	0.02	0.61
$\delta^{238}U$ vs. Mg/Ca (mol:mol)	0.05	0.35
$\delta^{238}U$ vs. $\delta^{18}O$	0.00	0.96
$\delta^{238}U$ vs. Sr concentration	0.05	0.37
$\delta^{238}U$ vs. Mn concentration	0.02	0.60
$\delta^{238}U$ vs. Mn/Sr	0.03	0.46
$\delta^{238}U$ vs. Mn/(Mg+Ca) (ppm/w.t.%)	0.05	0.83
$\delta^{238}U$ vs. Sr/(Mg+Ca) (ppm/w.t.%)	0.15	0.53
$\delta^{238}U$ vs. Ce anomalies	0.03	0.51
$\delta^{238}U$ vs. U/Al (ppm/w.t.%)	0.03	0.46
$\delta^{238}U$ vs. Al content	0.11	0.67
$\delta^{238}U$ vs. U/(Mg+Ca) (ppm/ wt.%)	0.17	0.48
$\delta^{238}U$ vs. Mo/(Mg+Ca) (ppm/ wt.%)	0.43	0.07
$\delta^{238}U$ vs. Mo/U	0.29	0.23
$\delta^{238}U$ vs. Fe/U (w.t.%/ppm)	0.07	0.27

Dengying and Yanjiahe Formation at Wuhe	R^2	p-value
$\delta^{238}U$ vs. Mg/Ca (mol:mol)	0.22	0.00
$\delta^{238}U$ vs. Ce anomalies	0.01	0.47
$\delta^{238}U$ vs. U/Al (ppm/w.t.%)	0.02	0.28
$\delta^{238}U$ vs. Fe/U (wt.%/ppm)	0.07	0.06

table S3. Summary of the parameters used in the modeling excise.

Parameter	Description	Values	Unit	References
J_{riv}	Riverine U fluxes to oceans	4.2×10^7	Mol/yr	(22),(54),(62),(94)
J_{oxic}	Removal flux to oxic sinks	2.23×10^7	Mol/yr	(22),(54),(62),(94)
$J_{suboxic}$	Removal flux to suboxic sinks	1.53×10^7	Mol/yr	(22),(54),(62),(94)
J_{anoxic}	Removal flux to anoxic sinks	4.45×10^7	Mol/yr	(22),(54),(62),(94)
k_{oxic}	Effective burial rate constant for oxic sinks	0.0536	dm/yr	(22)
$k_{suboxic}$	Effective burial rate constant for suboxic sinks	0.469	dm/yr	(22)
k_{anoxic}	Effective burial rate constant for anoxic sinks	0.939	dm/yr	(95–97)
$\delta^{238}U_{riv}$	$\delta^{238}U$ of river waters	−0.34	‰	(57)
$[U]_{modern}$	Modern seawater U concentration	1.39×10^{-8}	mol/dm^3	(23, 98)
$\delta^{238}U_{sw}$	Modern seawater $\delta^{238}U$	−0.4	‰	(23, 54)
Δ_{oxic}	Fractionation factor between oxic sink and seawater	0.005	‰	(23)
$\Delta_{suboxic}$	Fractionation factor between suboxic sink and seawater	0.1	‰	(54)
Δ_{anoxic}	Fractionation factor between anoxic sink and seawater	0.6	‰	(23, 24, 41, 42)
V	Seawater volume	1.37×10^{21}	dm^3	(99)
A	Total seafloor area	3.61×10^{16}	dm^2	(94)
	Modern anoxic seafloor area	0.35	%	(100)
	Modern suboxic seafloor aarea	6.00	%	(22)
	Modern oxic seafloor area	93.65	%	Balance